Hartmann–Shack wavefront reconstruction with bitmap image processing

Bezzubik, Vitalii; Belashenkov, Nikolai; Soloviev, Oleg; Vasilyev, Vladimir; Vdovin, Gleb

DOI
10.1364/OL.383464

Publication date
2020

Document Version
Final published version

Published in
Optics Letters

Optics Letters

Hartmann–Shack wavefront reconstruction with bitmap image processing

Vitalii Bezzubik,[1] Nikolai Belashenkov,[1] Oleg Soloviev,[1,2,3] Vladimir Vasilyev,[1] and Gleb Vdovin[1,2,3,*]

[1]ITMO University, Kronverksky 49, St. Petersburg, Russia
[2]TU Delft, Mekelweg 2, 2628CD, Delft, The Netherlands
[3]Flexible Optical BV, Polakweg 10-11, 2288GG Rijswijk, The Netherlands
*Corresponding author: gleb.vdovin@gmail.com

Received 18 November 2019; revised 3 January 2020; accepted 4 January 2020; posted 6 January 2020 (Doc. ID 383464); published 13 February 2020

In this Letter, we report on an algorithm and its implementation to reconstruct the wavefront as a continuous function from a bitmap image of the Hartmann–Shack pattern. The approach works with arbitrary raster geometry and does not require explicit spot definition and phase unwrapping. The system matrix, defining the coefficients of wavefront decomposition in the system of basis functions, is obtained as a result of a series of convolutions and thresholding operations on the reference and sample images.

https://doi.org/10.1364/OL.383464

Modal reconstruction of the wavefront $\varphi = \varphi(x, y)$ from the Hartmann–Shack (HS) data is performed in the form

$$\varphi = \sum_{i=1}^{N} a_i \psi_i, \tag{1}$$

where $\boldsymbol{a} = (a_1, \ldots, a_N)$ is the vector of coefficients, and $\{\psi_i\}$ is the set of basis functions. In practice, the basis functions ψ_i can be represented by δ functions defined in the nodes of a two-dimensional grid, resulting in zonal reconstruction [1,2]. The basis functions can have the form of trigonometric functions [3], Zernike polynomials, or Karhunen–Loeve functions for modal reconstruction [4]. In adaptive optical systems, the basis functions are presented by the influence functions of a wavefront corrector, usually a deformable mirror with N actuators [5].

The measurement principle used in this work is based on the registration of averaged wavefront tilts with the reconstruction performed in terms of continuous functions. Special processing methods for the detection of discontinuous and vortex wavefronts with the use of HS sensors [6] are not considered here.

The HS sensor encodes the information about the wavefront in the shifts $\boldsymbol{s}_j$ of the focal spots under the j-th subaperture A_j of the microlens array (MLA). Each of the shifts is proportional to a noisy measurement of the wavefront gradient, averaged over the j-th subaperture:

$$s_j \propto \int_{A_j} \nabla\varphi(x, y)\, \mathrm{d}x\mathrm{d}y + n_j$$

$$= \sum_i a_i \nabla_j \psi_i + n_j, \quad j = 1, \ldots J, \tag{2}$$

where $\boldsymbol{n} = (n_1, \ldots, n_J)$ denotes the measurement noise, and $\nabla_j \psi_i$ is a shorthand notation for the gradient of the i-th basis function, averaged over the j-th subaperture:

$$\nabla_j \psi_i \stackrel{\text{def}}{=} \int_{A_j} \nabla\psi_i(x, y)\mathrm{d}x\mathrm{d}y. \tag{3}$$

Assuming that the slopes measurement is affected by noise, the linear system of Eq. (2) can be solved by the least-squares method:

$$\hat{\boldsymbol{a}} = \arg\min_{\boldsymbol{a}} \sum_j \left| \boldsymbol{s}_j - \sum_i a_i \nabla_j \psi_i \right|^2, \tag{4}$$

which reduces to

$$\Psi \hat{\boldsymbol{a}} = \boldsymbol{b}, \tag{5}$$

with the elements of matrix Ψ and vector $\boldsymbol{b}$ given by

$$\Psi_{i,k} = \sum_j \langle \nabla_j \psi_i, \nabla_j \psi_k \rangle, \quad b_i = \sum_j \langle \nabla_j \psi_i, \boldsymbol{s}_j \rangle. \tag{6}$$

The expression for $\Psi_{i,k}$ is directly derived from Eq. (4), and the vector of coefficients b_i can be intuitively explained as the decomposition of the measured vector $\boldsymbol{s}$ over the set of derivatives of the basis functions $\nabla\psi_i$.

In this work, we set a goal to calculate all matrix components in Eq. (6) by performing purely bitmap operations on the intensity distributions registered by the HS sensor without any explicit definition of spot positions and their bounding boxes. To reach this goal, we first show how to use bitmap processing to calculate the x and y components of the displacement of the center of gravity (COG) of a single light spot. These displacements are proportional to the partial derivatives of the wavefront

in Eq. (2). Assume that in the absence of an aberration, the spot with intensity $I_0(x, y)$ is localized approximately in the centre of a circle C of radius A, specified as $\mathrm{circ}_A(x - x_0, y - y_0)$, where

$$\mathrm{circ}_A(x, y) = \begin{cases} 1 & x^2 + y^2 \le A^2 \\ 0 & \text{otherwise.} \end{cases} \tag{7}$$

If the intensity distribution of the displaced spot is denoted as $I(x, y)$, the shift $(\Delta x, \Delta y)$ of its COG restricted to area C is defined as [7]

$$\Delta x = \frac{\int_C I x \mathrm{d}x\mathrm{d}y}{\int_C I \mathrm{d}x\mathrm{d}y} - \frac{\int_C I_0 x \mathrm{d}x\mathrm{d}y}{\int_C I_0 \mathrm{d}x\mathrm{d}y},$$

$$\Delta y = \frac{\int_C I y \mathrm{d}x\mathrm{d}y}{\int_C I \mathrm{d}x\mathrm{d}y} - \frac{\int_C I_0 y \mathrm{d}x\mathrm{d}y}{\int_C I_0 \mathrm{d}x\mathrm{d}y}. \tag{8}$$

The result of Eq. (8) can be sampled at point (x_0, y_0) as the difference of ratios of two functions obtained from the intensity distributions convoluted with the top-hat function circ_A. The accuracy of Δx and Δy can be estimated as

$$\delta \sim \frac{p}{B} \frac{p^2}{\pi \rho^2}, \tag{9}$$

where p is the sensor pixel pitch, $\rho \gg p$ is the radius of the light spot on the sensor, and B is the signal-to-noise ratio of the sensor. For a spot that uses the whole dynamic range of the sensor, without saturation, the quantization noise prevails, and $B \approx 2^b/2$, where b is the sensor bit depth. For a standard 8-bit camera with a pixel pitch of $p = 5$ μm, spot radius of $\rho \approx 7$ μm, and $b = 8$ bit, we obtain the estimate for $\delta \approx 7$ nm.

Such sampling can be approximated with integration over a small region around the origin (x_0, y_0), defined by the selection mask function $S(x, y)$, which is set equal to 1 in the vicinity of the origin, and to 0 everywhere else. We define the mask as

$$S = \begin{cases} 1 & \frac{I_0}{\max(I_0)} \ge k_1 \frac{I_0 * \mathrm{circ}_A}{\max(I_0 * \mathrm{circ}_A)} \ \&\ I_0 > k_2 \max(I_0), \\ 0 & \text{otherwise.} \end{cases} \tag{10}$$

where & stands for logical "and," $k_1 \approx 1$ is the first thresholding coefficient defining the mask selectivity, and $0 < k_2 \le 1$ is the second thresholding coefficient serving to cut off spots with weak integral intensity. In our experiments, we used $k_1 = 0.95$, $k_2 = 0.2$. The value of k_1 should be maximized, and the value of k_2 minimized, to satisfy the condition that the majority of spots is detected within the aperture of interest. Expression (10) is a variant of classical blob detection procedure, described in more detail elsewhere (see for example [8]). Then the estimates to local derivatives can be defined by masking operation:

$$\Delta x(x, y) \approx S(x, y) \cdot \left(\frac{I x * \mathrm{circ}_A}{I * \mathrm{circ}_A} - \frac{I_0 x * \mathrm{circ}_A}{I_0 * \mathrm{circ}_A} \right),$$

$$\Delta y(x, y) \approx S(x, y) \cdot \left(\frac{I y * \mathrm{circ}_A}{I * \mathrm{circ}_A} - \frac{I_0 y * \mathrm{circ}_A}{I_0 * \mathrm{circ}_A} \right), \tag{11}$$

where $\cdot$ stands for a point-wise multiplication. Expressions [Eq. (11)] are valid if the pitch P is larger than the convolution kernel size A, and the expected spot shifts are smaller than A:

$$P > A > \sqrt{(\Delta x)^2_{\max} + (\Delta y)^2_{\max}}. \tag{12}$$

Expression (12) is satisfied in the majority of existing industrial HS sensors, where usually $A = P/2$, and the spot shifts are limited to the area of individual lenslet.

If the mask, defined by Eq. (10), identifies only one pixel per subaperture, the expression (11) provides the optimum precision because it is equivalent to the traditional COG algorithm [7]. However, for a mask that includes a number of pixels, the spot position is defined simultaneously in a number of shifted with respect to each other areas. Obviously, in this situation, the error due to finite mask size is negligible if the mask spot size is much smaller than the lenslet pitch.

Applying Eqs. (10) and (11) to the registered intensity distribution, one can calculate the fields of Δx and Δy over the whole area of the mask S. These fields can be directly used for calculation of the components of the system matrix in the right side of Eq. (5), corresponding to the sensor response to an unknown aberration. These components have meaning of scalar products of the spot displacements with the displacements produced by the basis functions:

$$\sum_j \langle \boldsymbol{s}_j, \nabla_j \psi_i \rangle \approx \frac{1}{F} \int_S \left(\Delta x \frac{\partial \psi_i}{\partial x} + \Delta y \frac{\partial \psi_i}{\partial y} \right) \mathrm{d}x\mathrm{d}y, \tag{13}$$

where Δx and Δy are defined by Eq. (11), and F is the focal length of the microlens array, or in the case of a Hartmann sensor, F is the distance from the Hartmann mask to the sensor.

The components of the left-side matrix Ψ in Eq. (5) can be calculated once for a system of basis functions, as element-wise cross-products of the masked derivatives of basis functions:

$$\sum_j \langle \nabla_j \psi_i, \nabla_j \psi_k \rangle \approx \int_S \langle \nabla \psi_i, \nabla \psi_k \rangle \mathrm{d}x\mathrm{d}y. \tag{14}$$

Expressions (13) and (14) allow to replace the scalar products of the spot shifts by integration over the whole area of the processed image, without any explicit definition of spot positions. To save the computation time, the gradients of the basis functions $\nabla \psi_i$, $i = 1, \ldots, N$ can be tabulated and stored in memory. The final integration over the mask area S, reduced to element-wise matrix multiplication, can be done after the reference spot pattern is registered, and the mask S is defined according to Eq. (10). These matrix operations can be easily vectorized for efficient implementation. Expressions [Eqs. (13) and (14)] completely define the system of linear equations [Eq. (5)] as a series of bitmap operations on the registered intensity distributions, and the set of basis functions.

Figure 1 illustrates the use of Eqs. (10) and (11) for the calculation of the spot displacement field for a simulated low-order HS pattern obtained for pure defocus. Both the mask S and the image describing the displacements of spots are obtained by bitmap operations on the input images, without any definition of vector entities, such as spot centers, localization areas, etc. All functions of these elements are taken over by the binary bitmap mask S.

For practical testing, we assembled a Michelson interferometer, schematic of which is shown in Fig. 2. The setup is formed by a reference flat mirror and deformable mirror, to facilitate testing of the setup with a variety of different aberrations. Two-arm setup allows to separate the registration of the HS patterns

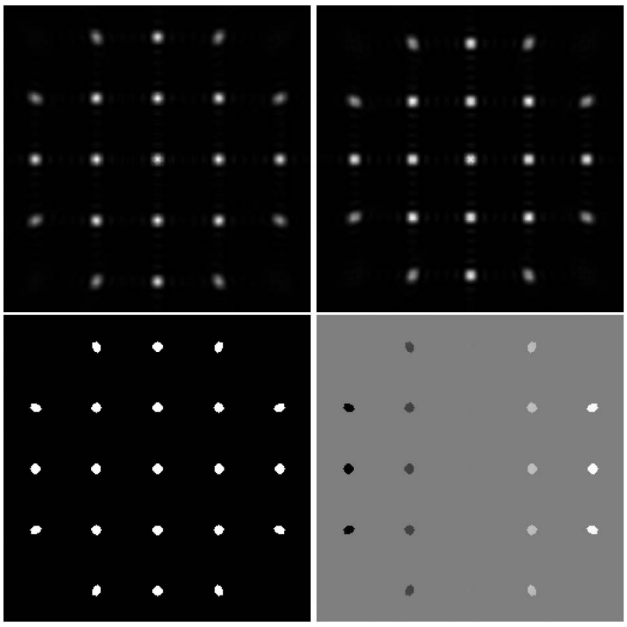

Fig. 1. Simulated reference (top left) and sample (top right) HS patterns, corresponding to pure defocus aberration. The mask S is generated according to Eq. 10 (bottom left), and the field of displacements Δy is reconstructed according to Eq. 11 (bottom right). Since the displacements are both positive and negative, the zero level is shown as gray in this image.

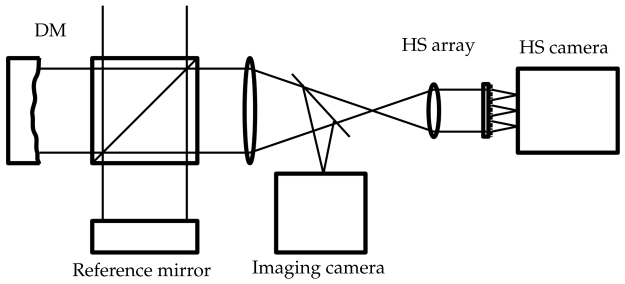

Fig. 2. Experimental interferometer for algorithm verification.

corresponding to the reference and sample wavefronts, by blocking the opposite arm of the interferometer. Also, the setup allowed registration of the interferometric pattern, corresponding to the aberration introduced by the deformable mirror, for independent method verification. The HS sensor was assembled with a microlens array MLA-150-5C (Thorlabs) with a pitch of 150 μm and a focal length of 4.1 mm with a grayscale camera UI-1540LE with a pixel pitch of ∼5.1 μm (produced by IDS imaging) having the 8-bit image depth. The full sensor aperture was formed by ∼1500 microlenses.

The reconstruction result, obtained on the basis of 177 Zernike polynomials, is shown in Fig. 3. The number of polynomials was chosen to be significantly smaller than the number of subapertures, to find the balance between the spatial bandwidth of the reconstruction, and the aliasing error due to regular periodic HS pattern [4]. The result demonstrates the stability of reconstruction and the ability of the algorithm to reconstruct the finest details of the object with an amplitude of a fraction of a wavelength.

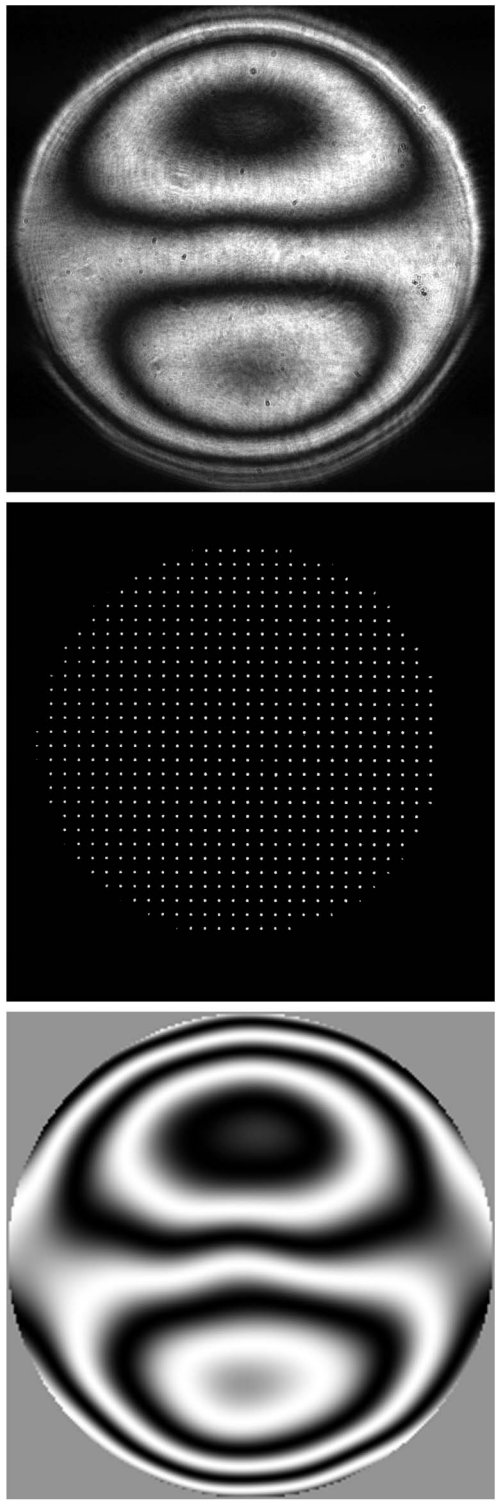

Fig. 3. Experimentally registered interferogram (top), matching an experimentally registered HS pattern (middle) of 1000 × 1024 pixels with 729 active spots, and its reconstruction (bottom) based on 177 Zernike polynomials. Note that the reconstruction is sensitive enough to reconstruct a low-amplitude high-frequency defect in the center of the object.

Mathematically, the convolution-based definition of spot positions is equivalent to the standard COG centroiding [7], with the elements of mask S defined as single pixels

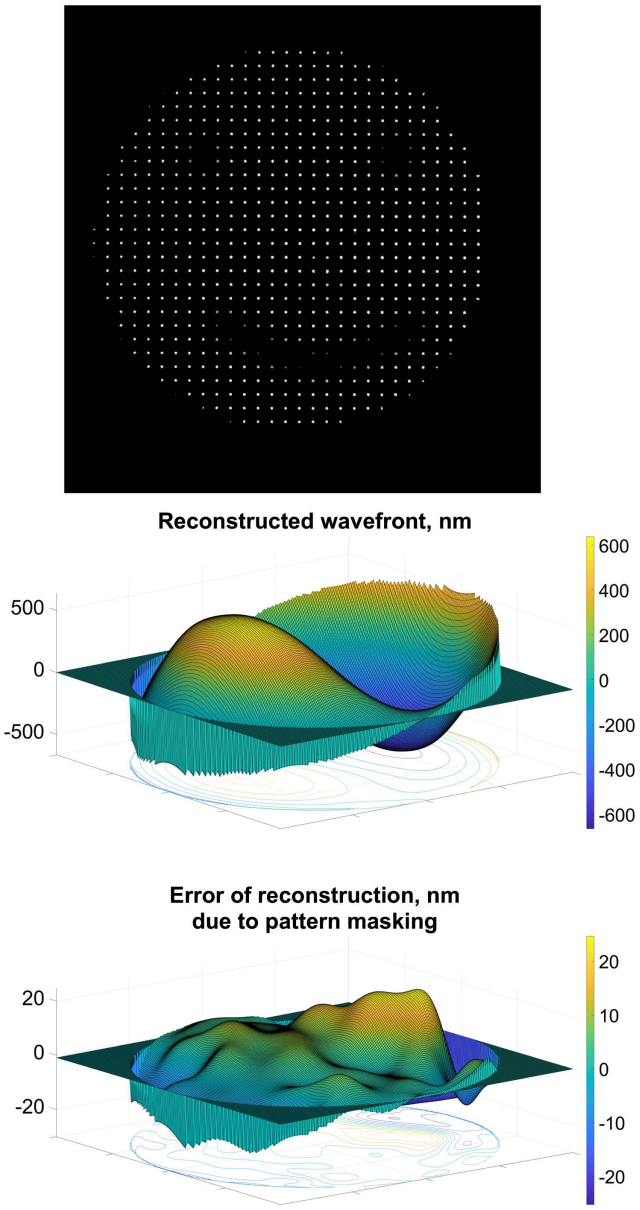

Fig. 4. Masked experimentally registered SH pattern, its reconstruction based on 177 Zernike polynomials, and reconstruction error (vertical scale enlarged 30 times) due to pattern masking. The *rms* reconstruction error due to masking does not exceed 8.1 nm, or $\sim \lambda/75$ for $\lambda = 633$ nm.

corresponding to delta functions centered at the lenslets. Since the mask definition Eq. (10) does not guarantee that the mask elements are formed by single pixels at the lenslet centroids, the COG model cannot be used to characterize the expected precision of reconstruction. Instead, the modified COG model should be used, in which the position of each centroid is defined as a COG position averaged over the area of corresponding mask element. The proposed method has a very useful property of self-calibrating adaptation of the mask geometry to real centroids, as they are presented in the reference pattern. This property allows implementation that works with practically any geometry of spot pattern, including pseudo-random configurations [4]. Since the positions and the quantity of spots are not predefined, the algorithm automatically adapts to the existing configuration of spot pattern in the field of view. The significant input parameters are the sensor pixel size and the distance from the mask (lenslet) to the image sensor and the minimum expected pitch of the lenslet P, limiting the size of convolution kernel A. Since the algorithm requires a reference image of the HS pattern, such an image should be registered experimentally with a reference surface, or calculated theoretically, based on the known parameters of the HS sensor. Figure 4 illustrates this property. We have masked some parts of the HS sensor pattern ($\sim$10% of all spots), both in the reference and sample images, and compared the result of reconstruction with the original, as shown in Fig. 3. The algorithm properly adapted to the change in the spot pattern, and it properly reconstructed the aberration. The resulting *rms* surface error caused by the masking 10% of spots, did not exceed $\lambda/75$.

The described method, representing a deep modification of the centroiding method [7], excludes explicit spot indexing and centroiding operation, making the reconstruction insensitive to spot indexing errors due to disappearing spots and spot data misinterpretation, especially for HS arrays with a large number of spots. The method also compares positively with the matching filtering method [3] as it does not include solving of an ill-posed problem of phase unwrapping.

In conclusion, in this Letter, we present an adaptive algorithm of wavefront reconstruction from the intensity data of a HS sensor, based on as a series of bitmap-image-processing operations. Unlike the majority of existing algorithms, our approach does not define spot positions as vectors, but instead, the components of reconstruction matrix are calculated directly in a series of bitmap operations. The algorithm is very simple in implementation. It can be used in the reconstruction of HS images with large numbers of spots and for masked and irregular HS patterns in optical quality control and industrial testing.

Funding. Ministry of Education and Science of the Russian Federation.

Disclosures. The authors declare no conflicts of interest.

REFERENCES

1. R. H. Hudgin, J. Opt. Soc. Am. **67**, 375 (1977).
2. D. L. Fried, J. Opt. Soc. Am. **67**, 370 (1977).
3. Y. Carmon and E. N. Ribak, Opt. Commun. **215**, 285 (2003).
4. O. Soloviev and G. Vdovin, Opt. Express **13**, 9570 (2005).
5. G. Vdovin, O. Soloviev, A. Samokhin, and M. Loktev, Opt. Express **16**, 2859 (2008).
6. K. Murphy and C. Dainty, Opt. Express **20**, 4988 (2012).
7. S. Thomas, T. Fusco, A. Tokovinin, M. Nicolle, V. Michau, and G. Rousset, Mon. Not. R. Astron. Soc. **371**, 323 (2006).
8. T. Lindeberg, *Scale-Space Theory in Computer Vision*, The Springer International Series in Engineering and Computer Science (Springer, 1993).